Original Research Article
ISSN: **3041-5357**
Journal homepage: https://diversity.researchfloor.org/

Journal of Diversity Studies

Sustainable Mycosynthesis of Silver Nanoparticles in Fruit Peel–Based Fungal Media: Characterization and Antimicrobial Applications

Pratima R Yadav*[1], and Rakesh U. Thakare[2]

[1]*Molecular Biology and Genetic Engineering Lab, Department of Microbiology, Rashtrasant Tukadoji Maharaj Nagpur University, Nagpur-440033, India*
[2]*Department of Microbiology, Yashwantrao Chavan College, Lakhandur, Dist. Bhandara, 441803, India*

ABSTRACT

Antimicrobial resistance among WHO priority pathogens (Escherichia coli, Pseudomonas aeruginosa, Enterococcus faecalis, and Staphylococcus aureus) and mounting fruit-peel waste demand sustainable solutions. Talaromyces-driven AgNP biosynthesis and peel-based nanoparticle production have each advanced separately; none has used the same peel waste as niche and cultivation matrix. Talaromyces strains OFA01 and MFA03, isolated from fruit-peel dumps onto peel-based agar, were grown in a composite four-peel broth (pomegranate : orange : mango : banana, 30 : 25 : 25 : 20 w/w) for AgNP biosynthesis. Optimum synthesis at 2 mM $AgNO_3$, pH 5, and 40 °C gave a clear SPR band at 415–420 nm with a peak absorbance of 0.696 AU. XRD confirmed face-centered-cubic crystalline silver with sharp reflections at 37.72°, 43.85°, 64.19°, and 77.03°; DLS gave a hydrodynamic diameter of 108.06 nm and a ζ-potential of −26.5 mV, indicating good colloidal stability. SEM micrograph analysis confirmed sub-spherical AgNPs with primary particle sizes of 30–80 nm, while the EDX spectrum displayed characteristic silver absorption peaks at ~3.0 keV and ~0.3 keV. Elemental mapping further demonstrated a uniform spatial distribution of silver across the sample, confirming high elemental purity and successful synthesis. FTIR, together with GC-MS profiling, identified proteins, phenolics, alcohols, and fatty-acid amides as agents serving simultaneously in reducing and capping roles. Against the four priority pathogens, MICs were 6.25–25 µg/mL (E. coli 6.25; E. faecalis 12.5; S. aureus and P. aeruginosa 25.0), with dose-dependent inhibition zones of 11.0–13.0 mm. The AgNPs synergized four antibiotic classes—gentamicin vs. E. faecalis (21.5 mm, +95.5%); ciprofloxacin vs. P. aeruginosa (25.0 mm, +47.1%); ampicillin vs. S. aureus (22.0 mm, +83.3%); and tetracycline vs. E. coli (28.5 mm, +23.9%)—and curbed F. oxysporum and A. alternata on par with amphotericin B. This first closed-loop integration of fruit-peel waste as a niche and cultivation medium offers a circular-economy route to AMR mitigation and crop protection.

Keywords: *Talaromyces; mycosynthesis; silver nanoparticles; fruit-peel waste; antibiotic synergism; Fusarium; Alternaria; circular economy.*

Citation: Pratima R Yadav, and Rakesh U. Thakare [2026]. Sustainable Mycosynthesis of Silver Nanoparticles in Fruit Peel-Based Fungal Media: Characterization and Antimicrobial Applications. *Journal of Diversity Studies.* **DOI: https://doi.org/10.51470/JOD.2026.5.2.30**

Corresponding Author: *Pratima R Yadav*

E-mail Address: *pratimesh093@gmail.com*

Article History: *Received 10 April 2026 | Revised 07 May 2026 | Accepted 12 June 2026 | Available Online July 09, 2026*

Copyright: *© 2026 by the author. The license of Journal of Diversity Studies. This article is an open access article distributed under the terms and conditions of the Creative Commons Attribution (CC BY) license* ***(https://creativecommons.org/licenses/by/4.0/).***

1. INTRODUCTION

Background and Significance

In recent years, nanotechnology has emerged as a transformative frontier in biological and material sciences, with metal-based nanoparticles occupying a central position in biomedical, environmental, and agricultural applications [1]. Among the various metallic nanoparticles, silver nanoparticles have attracted particular interest because of their broad-spectrum antimicrobial activity, high surface-area-to-volume ratio, and unique surface-plasmon resonance behavior [2, 3]. Conventionally, AgNPs are produced through physical and chemical routes that are energy-intensive, generate toxic by-products, and often produce particles with residual capping agents — limitations that have driven a paradigm shift towards greener, bio-inspired synthesis methods [1, 4].

Green and Mycosynthesis Approach

Biosynthesis employing plant extracts, bacteria, and especially fungi has now become the preferred route because biomolecules such as phenolics, flavonoids, terpenoids, proteins, and pigments act simultaneously as reducing and capping agents, producing stable, mono-dispersed nanoparticles under mild conditions [2, 5]. Fungi are particularly attractive bio-factories because their high biomass yield, tolerance to metal ions, and secretion of redox-active secondary metabolites enable reproducible, large-scale nanoparticle biosynthesis at industrial scales [2, 6]. Fungal pigments — notably the polyketide-derived red pigments of *Talaromyces* spp. — have further been shown to convert Ag^+ to Ag^0 cleanly under ambient conditions, including sunlight [7].

The Talaromyces Genus as a Versatile Nano-Factory

Among filamentous fungi, the genus *Talaromyces* has, in the last few years, been consistently highlighted as a prolific producer of biogenic AgNPs. *T. funiculosus* biosynthesis, for example, yields spherical monodispersed AgNPs of average diameter 34.32 nm with ζ-potential of −18.41 mV, IC_{50} values of 48.11 ppm and 35.88 ppm, and MICs of 3.7 µg/mL against *Escherichia coli* [2].

T. purpureogenus isolated as an endophyte produces AgNPs with spherical and triangular morphologies and an MIC of 16.12 µg/mL against *Staphylococcus aureus* [8]. Extracellular pigment of *T. purpurogenus* yields 4–41 nm AgNPs with SPR ~410 nm, ζ-potential of −24.8 mV, and MICs of 32 µg/mL (*E. coli*) and 4 µg/mL (*S. epidermidis*) [3]. *T. australis* pigment under solar irradiation forms 16 ± 2 nm FCC-crystalline AgNPs with antibacterial MICs as low as 62.5 µg/mL, DPPH/ABTS IC_{50} <10 µg/mL and HeLa GI_{50} <10 µg/mL [7]. *T. islandicus* VSGF1 has been reported to yield 13–66 nm AgNPs with ZOIs up to 18.66 ± 0.57 mm against drug-resistant *Enterococcus faecalis* and an MTT IC_{50} of 38.17 µg/mL against HepG2 [6]. *T. stipitatus* has also been optimized via response surface methodology for AgNP biosynthesis active against *S. aureus*, *B. cereus*, *P. aeruginosa*, *K. pneumoniae*, *Aspergillus flavus*, *A. niger*, *F. oxysporum*, and *Alternaria alternata* [13]. Taken together, these reports establish *Talaromyces* as a genus with consistent, multi-attribute biomedical performance.

Fruit-Peel Waste as Both Niche and Feedstock

Parallel to the rise of biogenic AgNPs, the global agro-industrial disposal of fruit peels has emerged as a parallel grand challenge. It is estimated that a substantial fraction of processed fruit mass — peels and rinds — is discarded as waste despite being rich in phenols, flavonoids, tannins, triterpenoids, carotenoids, ellagitannins, vitamin C, and essential oils [5]. This waste stream is increasingly being valorised: peels of *Citrus sinensis*, *Citrus limon*, *Musa paradisiaca*, *Mangifera indica*, and *Punica granatum* have all been converted into AgNP-generating matrices that produce spherical particles of 10–75 nm with significant antimicrobial activity [4, 9, 10]. A 2021 review concluded that biowaste-fabricated AgNPs represent a sustainable, low-cost platform for antimicrobial coatings in biomedicine [11].

Antimicrobial Resistance — Why Antibiotic-Synergism Matters

The clinical urgency underpinning this work is the continuing escalation of antimicrobial resistance. The WHO has repeatedly flagged *Enterococcus faecalis*, *Pseudomonas aeruginosa*, *Staphylococcus aureus*, and *Escherichia coli* as priority pathogens for which novel therapeutic adjuvants are urgently needed [2, 6]. Importantly, biogenic AgNPs restore or even enhance the activity of failing antibiotics through membrane permeabilization and reactive-oxygen-species generation; reports of AgNP–antibiotic synergy against MDR clinical isolates now exist for lignin-degrading fungal systems [12] and for AgNPs combined with gentamicin, ciprofloxacin, ampicillin, and tetracycline against standard ATCC strains [2]. Furthermore, fungal phytopathogens such as *Fusarium oxysporum* and *Alternaria alternata* cause massive post-harvest losses worldwide, and AgNPs derived from peel matrices have shown promising antidermatophytic activity [4, 13].

Research Gap and Hypothesis

Despite the expanding literature on *Talaromyces*-mediated AgNP synthesis [2, 3, 6, 8, 13], the parallel growth of fruit-peel valorization for nanomaterial production [4, 5, 9, 11], a critical gap remains: no previous study has utilized the same fruit peel waste both as the isolation niche and as the cultivation matrix for *Talaromyces*-mediated AgNP biosynthesis nor evaluated such AgNPs against bacterial and phytopathogenic targets conjointly with multiple classes of conventional antibiotics.

Hypothesis. Metallotolerant, pigment-producing *Talaromyces* spp. resident in fruit-peel disposal sites can be isolated, propagated directly on the same peel-derived broth, and used to biogenic-produce AgNPs exhibiting (a) low MICs against priority bacterial pathogens, (b) significant antiphytopathogenic activity, and (c) synergy with at least one antibiotic from each of the aminoglycoside, fluoroquinolone, β-lactam, and tetracycline classes.

Objectives

This work aims to investigate the eco-friendly biosynthesis of silver nanoparticles (AgNPs) using Ascomycetes isolated from waste dump sites and grown on fruit peel based culture media. After structural and optical characterization using UV–vis spectrophotometry, SEM, XRD and FTIR, antimicrobial potential of the biogenic AgNPs was analyzed comprehensively in comparison to the commonly used antibiotics which are targeted against the multidrug resistant (MDR) bacteria and phytopathogenic fungi.

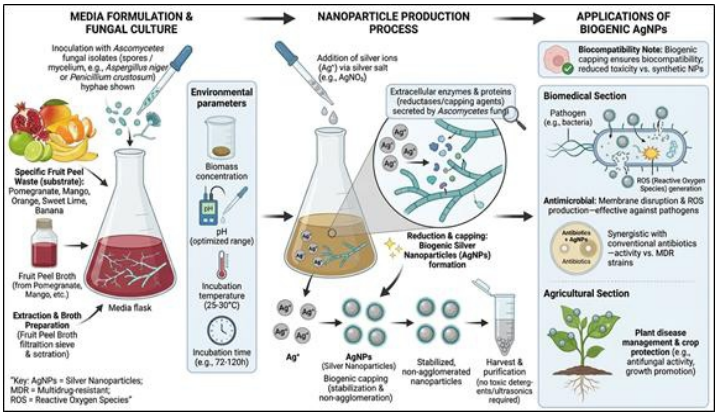

Image: Schematic Representation of Synthesis of Silver nanoparticles from Agrowaste

To the best of our knowledge, this is the first study to integrate fruit-peel waste as both the isolation niche and the cultivation matrix for *Talaromyces*-mediated AgNP biosynthesis, with standardized parameters with conjoint evaluation of bactericidal activity against four WHO priority pathogens, antibiotic-adjuvant synergy across four drug classes, and antifungal potential against *F. oxysporum* and *A. alternata*.

2. MATERIAL AND METHOD

2.1 Sample Collection and Media Preparation

Fruit peel waste was collected from local vendor dump sites in Nagpur district, Maharashtra, India. Five peel types—*Citrus sinensis* (sweet orange), *Musa paradisiaca* (banana), *Punica granatum* (pomegranate), *Citrus limetta* (sweet lime), and *Mangifera indica* (mango)—were procured in sterile polythene bags, transported to the laboratory within 2 h, and processed immediately. The peels were rinsed thrice with tap water followed by distilled water to remove adhering debris and surface contaminants [4,9].

Individual peel powders or a blend of four peels (pomegranate:orange:mango:banana) in a 30:25:25:20 w/w ratio were suspended in double-distilled water and stirred at 60 °C for 30 min followed by filtration. Filtrate pH was adjusted to the range of 5.5–6.5 by using 0.1 M NaOH. This solution was directly used as a fruit peel broth for biomass cultivation, and 2% (w/v) agar-agar was added to it and autoclaved (121 °C, 15 psi, 15–20 min) to obtain fruit peel agar plates for isolate cultivation.

The switch from synthetic to peel-based media reflects the sustainable green-synthesis model that opts for polyphenol-rich plant nutrients in place of peptone- or yeast-extract–based formulations, thereby reducing cost and environmental burden [1,4,9].

2.2 Isolation and Morphological Screening of Fungi on FPA

Approximately 1 g of decomposed peel material was suspended in 9 mL of sterile physiological saline (0.85% NaCl), vortexed for 2 min, and serially diluted up to 10^{-4}. Aliquots (100 µL) from each dilution were spread-plated onto freshly prepared FPA plates amended with streptomycin (100 µg mL^{-1}) to suppress bacterial growth. Plates were incubated at 25 ± 2 °C for 5–7 days and observed daily for colony emergence [2,14]. Morphologically distinct colonies were sub-cultured onto fresh FPA plates to obtain pure cultures. Pigment-producing colonies—green, grey-green, or black—were preferentially picked, since pigment secretion has consistently correlated with extracellular Ag^+ reduction efficiency in *Talaromyces* spp [3,7].

2.3 ITS-Based Identification of Isolates

Two pigment-producing strains—designated *Talaromyces* sp. OFA01 (from orange peel) and *Talaromyces* sp. MFA03 (from mango peel) was selected for further work. Mycelia from 5-day-old cultures were used for genomic DNA isolation by the CTAB method. Purity and concentration were confirmed by 1% agarose gel electrophoresis. The internal transcribed spacer region was amplified using universal primers ITS1 (5′–TCCGTAGGTGAACCTGCGG–3′) and ITS4 (5′–TCCTCCGCTTATTGATATGC–3′) [2,8]. Amplicons were sequenced, and the resulting contigs were compared against the NCBI GenBank database using BLASTn.

2.4 Cultivation of Isolated Strain in Peel-Derived Broth

A stock culture of the *Talaromyces* strain OFA01 was selected for subculturing separately into 100 mL of sterile fruit-peel liquid broth (Section 2.1) due to more biomass production. Incubation was performed on a rotary shaker at 25 ± 2 °C, 120 rpm, for 4–5 days to facilitate mycelial development [2, 8]. Fungal biomass was harvested by filtration through double-layered muslin cloth, washed thrice with sterile distilled water, and resuspended in distilled water for 24–48 h to release extracellular proteins and metabolites required for metal-ion reduction [14, 15].

2.5 Fungal Biosynthesis of Silver Nanoparticles

A 100-mL aliquot of 2 mM silver nitrate solution was added to 100 mL of cell-free fungal filtrate (1:1 v/v), giving a final reaction volume of 200 mL. The mixture was incubated in the dark at 40 ± 2 °C to prevent photo-reduction, ensuring that nanoparticle formation is mediated entirely by fungal enzymes and pigments [3, 8]. A visible color shift from pale yellow to reddish-brown within 4 hrs indicated surface-plasmon-resonance excitation and successful AgNP formation [2,8]. For purification, the reaction mixture was centrifuged at 10,000 × g for 15 min, the pellet was washed three times with sterile distilled water and once with absolute ethanol to remove unbound biomolecules, and the final pellet was dried in a hot air oven. Dried AgNP powder was stored in amber vials at 4 °C in the dark [8].

Negative Controls

Reactions under identical conditions but containing (a) cell-free filtrate without $AgNO_3$ and (b) 2 mM $AgNO_3$ without filtrate were maintained in parallel as negative controls. Both controls remained colorless throughout the incubation period, confirming the role of fungal secretions in Ag^+ reduction.

2.6 Optimization of Synthesis Parameters

Synthesis was optimized by varying one parameter at a time while keeping the others fixed:

- $AgNO_3$ concentration: 0.5, 1, 2, 3, mM
- pH: 5, 6, 7, 8
- Temperature: 28, 40, 50, 60 °C

Each parameter's influence on synthesis kinetics and final particle size was monitored by UV-visible spectrophotometry at 420 nm. The narrowest absorbance band centered at 415–420 nm will be used to define the optimum [2, 8, 20].

2.7 Physicochemical Characterization

2.7.1 UV-Visible Spectroscopy

SPR spectra were recorded on a UV-Vis spectrophotometer in the 300–700 nm range against a distilled water blank. The peak wavelength (λmax) and absorbance served as primary confirmation of AgNP formation [2, 8].

2.7.2 Scanning Electron Microscopy and Energy-Dispersive X-ray Spectroscopy

Lyophilized AgNPs were re-dispersed in distilled water, drop-cast onto carbon tape, and air-dried. Samples were gold-sputter-coated (~10 nm) prior to imaging at 5–15 kV accelerating voltage. EDS spectra were acquired to confirm the elemental Ag signal at 3.0 keV [2] .

2.7.3 X-Ray Diffraction

XRD was performed on lyophilized AgNP powder using Cu Kα radiation (λ = 1.5406 Å) at 40 kV / 30 mA in the 2θ = 30–80° range. Bragg reflections corresponding to the planes of face-centered cubic silver were indexed to confirm crystallinity [2, 3].

2.7.4 Fourier-Transform Infrared Spectroscopy

FTIR spectra were recorded over 4000–400 cm^{-1} at a resolution of 4 cm^{-1} using the KBr pellet method. Peaks diagnostic of O–H stretches (≈ 3400 cm^{-1}), amide N–H bands (≈ 1640 cm^{-1}), and aromatic or carboxyl C=O (≈ 1400 cm^{-1}) confirmed protein/phenolic capping on the AgNP surface [2, 8].

2.7.5 Dynamic Light Scattering and Zeta Potential

Hydrodynamic diameter, polydispersity index, and zeta potential were measured on a Malvern Zetasizer at 25 °C using disposable folded capillary cuvettes. Samples were diluted 1:10 with double-distilled water; measurements were taken in triplicate and expressed as mean ± SD [2, 19].

2.7.6 GC-MS Analysis of Mycogenic Extract

The cell-free filtrate was partitioned with ethyl acetate (1:1 v/v), dried over anhydrous Na_2SO_4, and analyzed on a GC-MS system fitted with a DB-5MS capillary column (30 m × 0.25 mm × 0.25 µm) using He as carrier gas. Compounds were identified by matching mass spectra against the NIST library (≥ 80 % similarity threshold) [2, 8].

2.8 Antimicrobial Assays

2.8.1 Test Organisms

Gram-positive and Gram-negative priority pathogens were obtained from MTCC, Pune, India. The panel included:

- Gram-positive: *Staphylococcus aureus* MTCC 96, *Enterococcus faecalis* MTCC 439
- Gram-negative: *Escherichia coli* MTCC 1687, *Pseudomonas aeruginosa* MTCC 1688
- Plant pathogens (antifungal evaluation): *Fusarium oxysporum* MTCC 284 and *Alternaria alternata* MTCC 1360

2.8.2 Zone-of-Inhibition — Disc Diffusion

ZOI was assessed by the Kirby–Bauer disc-diffusion method on Mueller–Hinton agar plates pre-inoculated with a 0.5 McFarland-adjusted test suspension (~1.5 × 10^8 CFU mL^{-1}). Sterile 6-mm discs were impregnated with 20 µL of serial AgNP dilutions (10, 25, 50, 75, 100 µg $disc^{-1}$). Plates were incubated at 37 ± 1 °C for 18–24 h, and diameters of the inhibition zones (mm) were measured. Standard antibiotic discs (ampicillin 10 µg, ciprofloxacin 5 µg, tetracycline 30 µg, gentamicin 120 µg) served as positive controls [8, 17, 21].

2.8.3 Minimum Inhibitory Concentration — Broth Microdilution

MIC was determined in 96-well microtitre plates following CLSI guidelines. Two-fold serial dilutions of AgNPs (100 → 3.125 µg mL^{-1}) were prepared in MH broth, and each well was inoculated with 100 µL of bacterial suspension adjusted to 0.5 McFarland. Plates were incubated at 37 °C for 18–24 h; the lowest concentration showing no visible turbidity was recorded as the MIC. All experiments were performed in triplicate, and results were expressed as mean ± SD. Negative (broth only) and positive (gentamicin dilution series) controls were included [2, 17].

2.8.4 Antibiotic Synergy Assay

AgNP–antibiotic combinations were evaluated by the disc-diffusion method using a checkerboard-style overlay. Standard antibiotic discs (gentamicin 120 µg, ciprofloxacin 5 µg, ampicillin 10 µg, tetracycline 30 µg) were placed on Mueller–Hinton agar pre-inoculated with the test organism, and AgNP dilutions (10, 25, 50, 75, 100 µg $disc^{-1}$) were added on top of each antibiotic disc. The simultaneous application allowed diffusion of both agents. Plates were incubated at 37 ± 1 °C for 24 h, and ZOI diameters were measured. Synergism was defined as a ≥ 5 mm increase in ZOI over the antibiotic-alone baseline; additivity as a 1–4 mm increase; and indifference as no change [2, 16, 17].

2.8.5 Antifungal Assay

Antifungal efficacy was evaluated against *F. oxysporum* and *A. alternata* by disc diffusion on potato-dextrose agar plates pre-inoculated with 6-mm mycelial discs from 7-day-old cultures. Each AgNP dilution was loaded onto sterile discs and placed equidistantly; 25 µg amphotericin B served as the positive control [18]. Plates were incubated at 28 ± 1 °C for 6 days, and ZOI diameters (mm) were recorded on day 7.

3. RESULT AND DISCUSSION

3.1 Fungal Identification and Morphological Analysis

Two pigment-producing isolates (OFA01 and MFA03) were recovered on fruit peel agar (25 ± 2 °C, 5–7 days). OFA01 gave a series of olive-green sporulation sectors in granular colonies, while MFA03 gave cottony, dark-grey colonies.

Both strains had typical *Talaromyces* architecture when examined under the microscope: hyaline hyphae, biverticillate conidiophores, flask-shaped phialides, and catenulate, cylindrical conidia. There were also inclusions of brown granules and occasional monoverticillate structures observed in MFA03. Genetic differentiation was determined by ITS rDNA sequencing (ITS1/ITS4) and BLASTn search. The ~612 bp sequence of OFA01 (GenBank: PX475677) was 95.31% identical to *Talaromyces* sp. XMSF-1, whereas the ~599 bp sequence of MFA03 (GenBank: PX475678) shared 99.32% identity with strain MT141150.1. Neighbor-joining phylogenetic trees also showed that OFA01 grouped with *T. funiculosus* and MFA03 placing adjacent to endophytic *T. purpureogenus* and *T. islandicus* [6].

Fig. 1. ITS-based phylogenetic placement of Talaromyces sp. OFA01 and Talaromyces sp. MFA03 within the genus Talaromyces

3.2 Evaluation of FPB Media for Fungal Cultivation

The composite four-peel blend broth was used to evaluate cultivation profiles (pomegranate/orange/mango/banana 30:25:25:20 w/w, 20 rpm, 25 ± 2 °C for 4–5 days) and indicated that isolate OFA01 produced higher mycelial mass and darker cell-free filtrate than MFA03, suggesting that isolate OFA01 is the promising one to be optimized. This improved secretory and growth ability is attributed to the synergic polyphenolic and carbohydrate matrix of the mixed peel, which maintains constant C:N ratios without substrate poisoning [9]. This multi-waste stream can lower production costs and reduce the environmental footprint when replacing the synthetic media [9, 15].

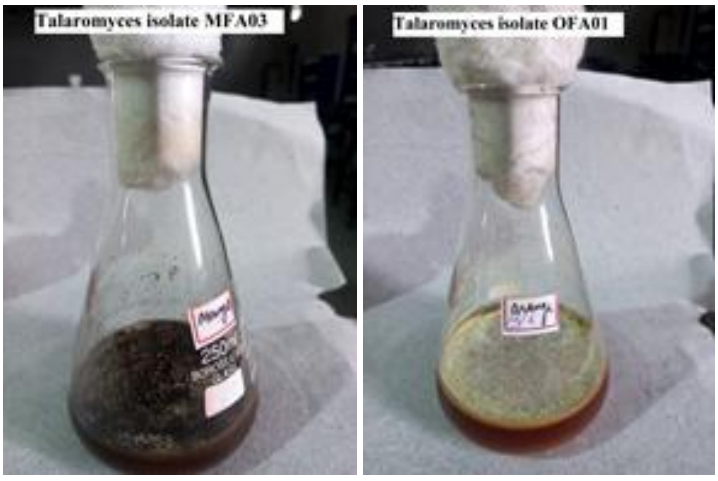

Fig. 2. Biomass of Talaromyces sp. OFA01 and MFA03 grown in orange-peel and mango-peel broth after 4–5 days of incubation at 25 ± 2 °C, 120 rpm]

3.3 Optimization of Silver-Nanoparticle Synthesis

Synthesis of AgNPs from OFA01 orange-peel filtrate was monitored by UV-Vis spectroscopy. Within 30–90 min of adding 2 mM $AgNO_3$ to the cell-free filtrate (1:1 v/v, pH 5, 40 °C, dark incubation), the reaction mixture turned from pale yellow to

reddish-brown—the classical SPR signature of $Ag^{+} \rightarrow Ag^{0}$ reduction [3, 8]. Importantly, the dual negative controls—filtrate-only and $AgNO_3$-only under identical conditions—remained colorless, confirming that AgNP formation was driven by fungal enzymes/redox metabolites rather than by photolysis or spontaneous nucleation.

Table 1: Variation of the three primary thermodynamic inputs produced the following optimum

Parameter	Range tested	Optimum for OFA01	Closest literature data point
$AgNO_3$ (mM)	0.5–3	2	*T. funiculosus* optimum 2 mM [3]; *T. stipitatus* RSM optimum 2 mM [9]
pH	3–8	5	*T. purpureogenus* optimum ~7 [8]; *T. purpurogenus* pH 7–9 [2]
Temperature (°C)	25–50	40	*T. stipitatus* 30 °C [9]; *T. purpureogenus* 28 °C [8]; *T. funiculosus* 40 °C [3]

The acidic optimum (pH 5) is therefore thermodynamically preset by the broth itself since mixed fruit peel has pH 4.5–5.5 [9]. This means the closed-loop system already operates at its own thermodynamic optimum, eliminating external buffering—a process-integration parameter that, to our knowledge, has not been explicitly demonstrated in the *Talaromyces*-AgNP literature to date.

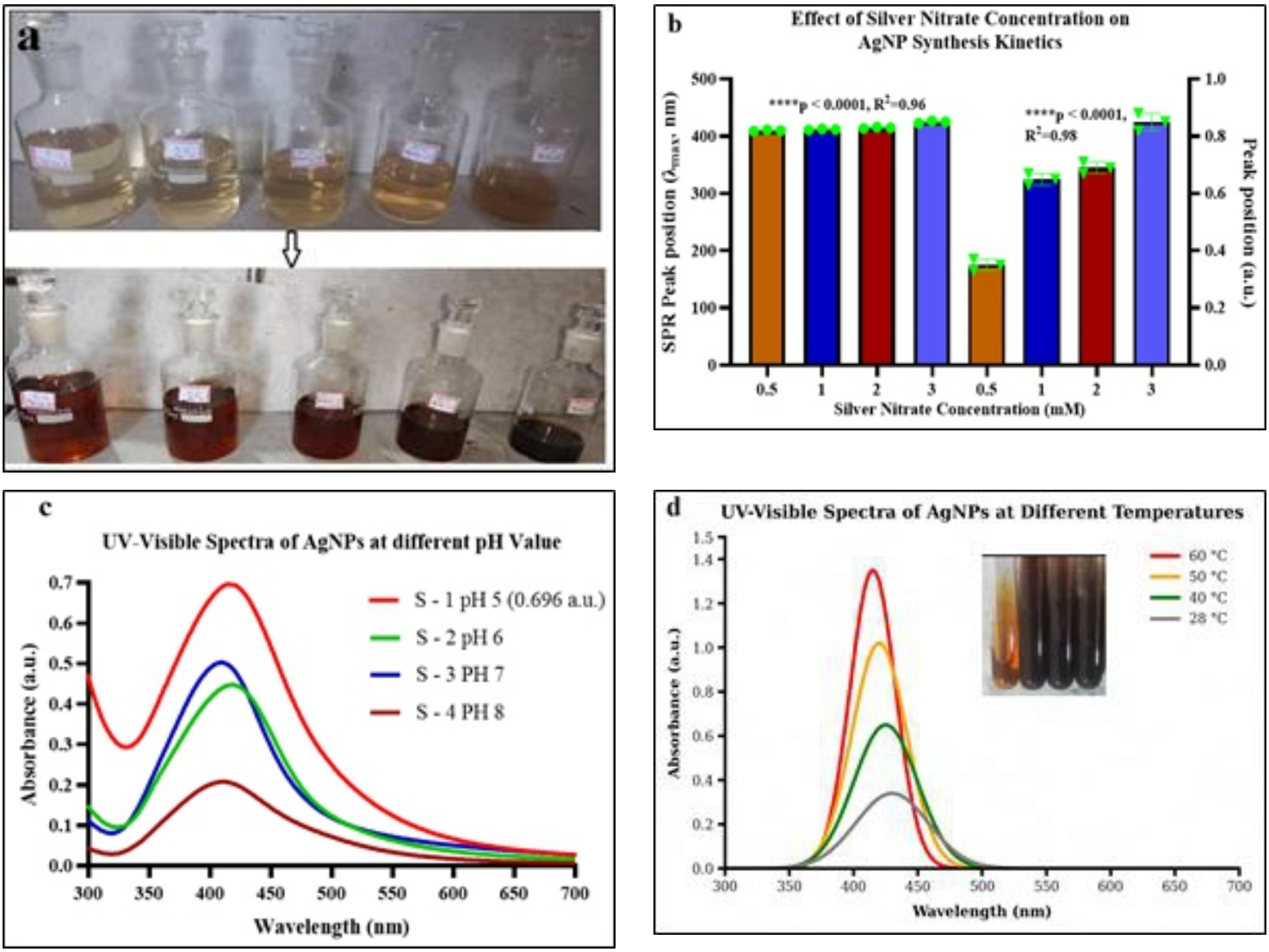

Fig. 3. Optimization of biosynthesized AgNPs: (a) combined effect of synthesis parameters; (b) effect of $AgNO_3$; (c) effect of pH; (d) Effect of temperature]

3.4 Physicochemical Characterization of AgNPs

3.4.1 UV-Visible Spectroscopy

The sharp SPR band at 415–420 nm with absorbance 0.696 AU indicates predominantly spherical (Fig. 4a), monodisperse AgNPs and is congruent with the SPR maxima reported for *T. funiculosus* (≈ 420 nm) [12], *T. purpurogenus* pigment-AgNPs (≈ 410 nm) [3], *T. australis* solar-route AgNPs [7], and the consensus 415–430 nm window for biogenic AgNPs generally [12].

3.4.2 SEM and EDX

The SEM micrograph image confirms the formation of sub-spherical silver nanoparticles with a primary particle size ranging from 30 nm to 80 nm. The EDX spectrum shows strong characteristic peaks corresponding to the optical absorption of metallic silver at ~3.0 keV and ~0.3 keV consistent with previous results of *Talaromyces*-mediated AgNPs [2], confirming strong secretome-driven reduction kinetics. In addition, elemental mapping shows that Ag is present in a uniform spatial distribution across the sample, indicating good elemental purity and successful synthesis.

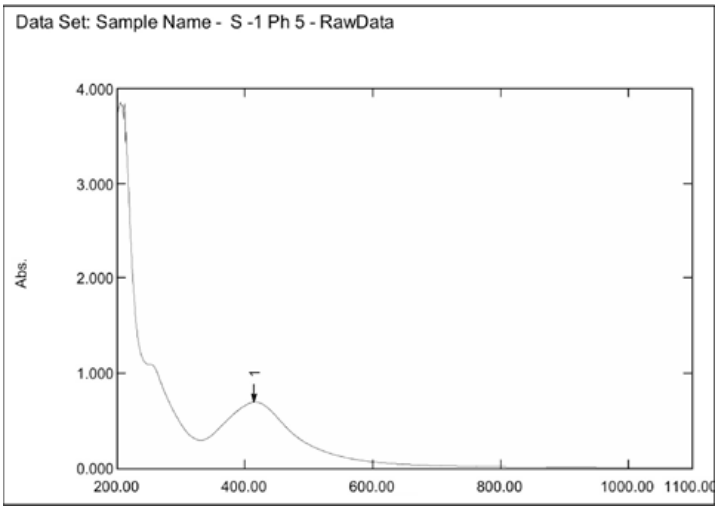

Fig 4a: UV Spectrum of AgNPs

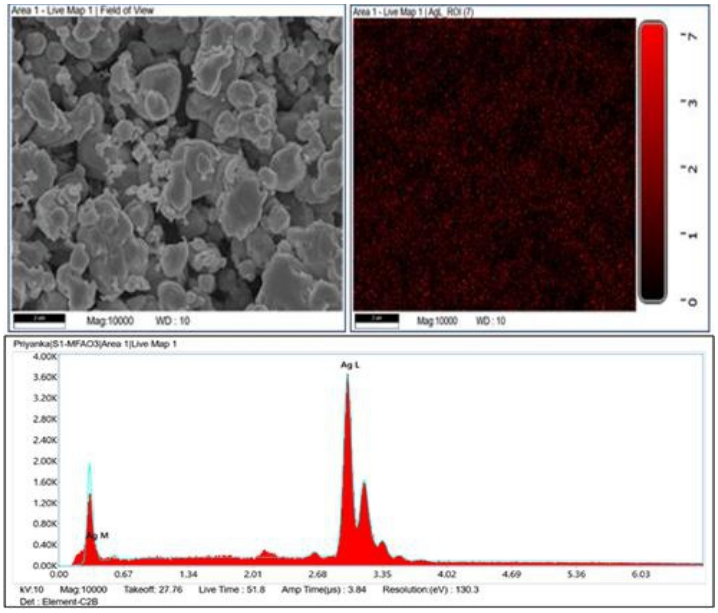

Fig 4b: SEM EDX of AgNPs

3.4.3 XRD Spectrum

X-ray diffraction showed the four sublime reflections at 2θ = 37.72°, 43.85°, 64.19°, and 77.03°, indexing to the planes of face-centered-cubic crystalline silver (Fig. 4c). The pattern mirrors the FCC profiles obtained for *T. funiculosus* [2], *T. purpurogenus* [3], and *T. islandicus* VSGF1 [6]; the absence of parasitic oxide reflections confirms the high purity of the recovered AgNPs.

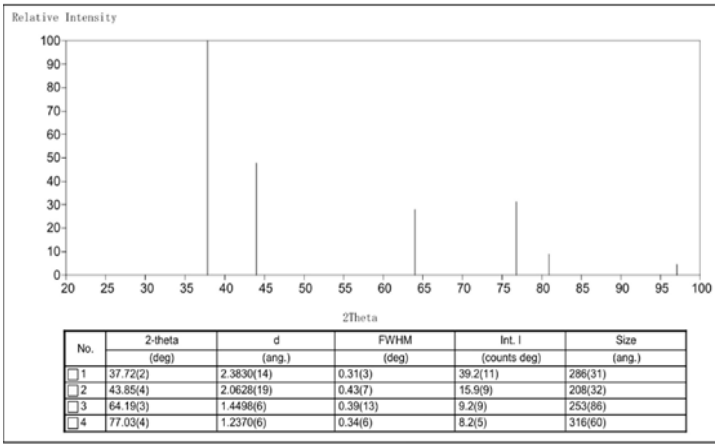

No.	2-theta (deg)	d (ang.)	FWHM (deg)	Int. I (counts deg)	Size (ang.)
1	37.72(2)	2.3830(14)	0.31(3)	39.2(11)	286(31)
2	43.85(4)	2.0628(19)	0.43(7)	15.9(9)	208(32)
3	64.19(3)	1.4498(6)	0.39(13)	9.2(9)	253(86)
4	77.03(4)	1.2370(6)	0.34(6)	8.2(5)	316(60)

c) XRD spectra

3.4.4 FTIR

FTIR analyses revealed diagnostic O–H (~ 3400 cm^{-1}), C=O (~ 1640 cm^{-1}), and C–N (~ 1400 cm^{-1}) bands—i.e., amide-I/II regions typical of proteinaceous capping combined with phenolics/alcohols (Fig. 4d). The fingerprint closely matches the FTIR profile reported for *T. purpureogenus* endophyte AgNPs [8], *T. funiculosus* AgNPs [2], and lignin-degrading fungal AgNPs [12].

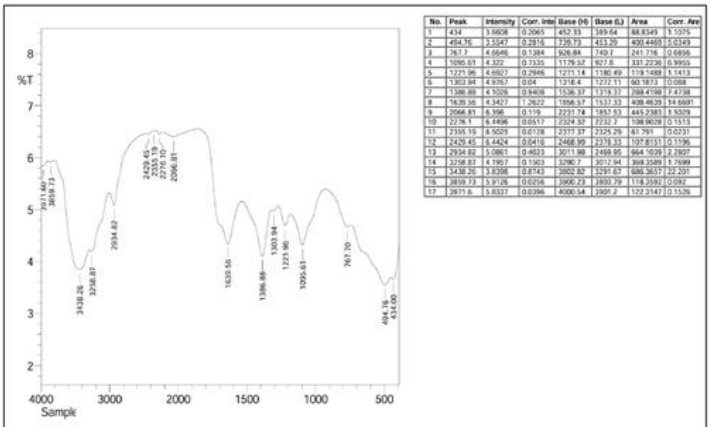

d) FTIR spectrum

3.4.5 DLS and Zeta Potential

The monomodal OFA01 AgNPs obtained from the DLS analysis showed a peak diameter of 108.06 nm with a low PDI of 25.7% (Fig. 4e). The average zeta potential found for the nanoparticles was a net negative value of −26.5 mV with a peak value of −22 mV (Fig. 4f), which is consistent with the findings of other studies on *Trichoderma* mycosynthesis reported previously [22, 23]. This charge is generated through matrix deprotonation by fungi, which provides strong electrostatic repulsive energy and colloidal stability despite low double-layer compressibility associated with the low conductivity of the solution, 1.531 mS/cm.

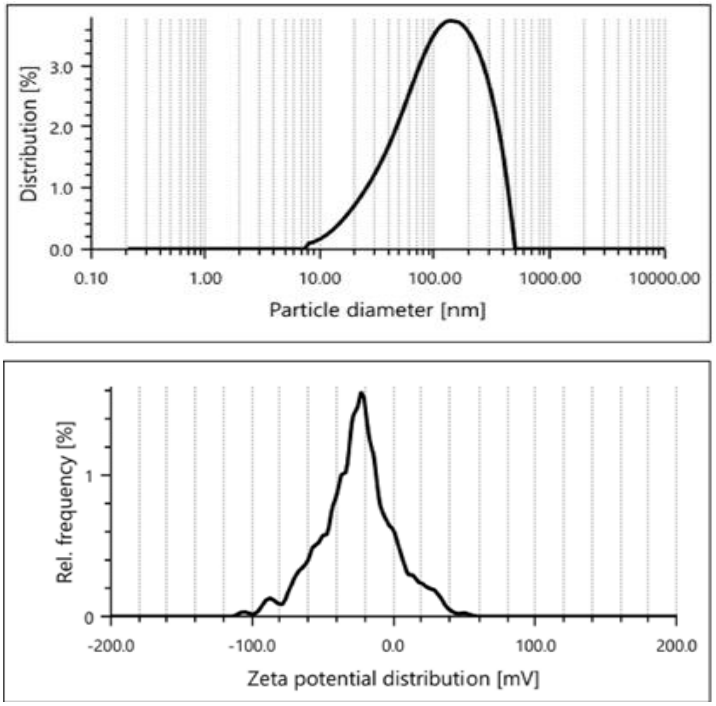

Fig 4e) DLS; Fig 4f) Zeta Potential

3.4.6 GC-MS Analysis of Mycogenic Extract

GC-MS profiling of the ethyl-acetate partition revealed a metabolite window spread over RT 3.42–43.18 min and dominated by alcohols, fatty-acid amides, and siloxane derivatives, with the dominant feature at RT 37.66 bearing a peak area of 1.38 × 10^9 (Fig. 4g). This is consistent with the polyketide/pigment-class reductants documented for *T. purpurogenus* [3] and *T. funiculosus* [2], both of which similarly rely on alcohol/amide-type secondary metabolites as Ag^+-reducing suffragans. Mechanistically, the small-molecule reductant profile complements the proteinaceous fingerprint, explaining why OFA01 reduces Ag^+ to Ag^0 in less than 90 min—faster than the typical 2–6 h reduction time of plant-extract–mediated syntheses [4, 9] and on a par with algal-marine fungal biogenic syntheses [19].

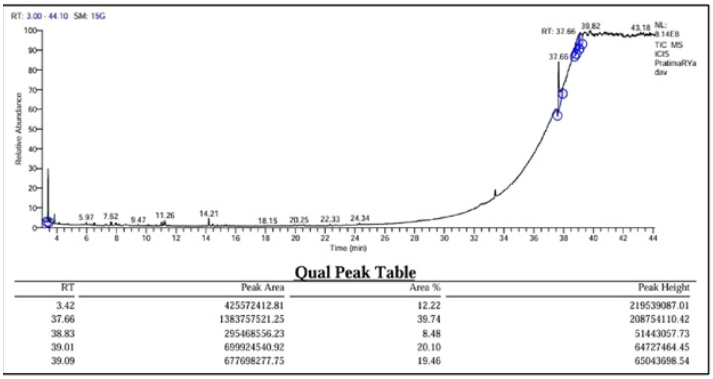

Fig 4g) GCMS spectra

3.5 Antimicrobial Activity of OFA01-AgNPs

3.5.1 Antibacterial Potential and Comparative Synergism

The ZOI diameters of antimicrobial activity and antibiotic OFA01-AgNPs were recorded as 11.0–13.0 mm for all the priority pathogens used, and inhibition was detected up to 10 µg $disc^{-1}$, corresponding to a 6.5–8.0 mm ZOI diameter. High potency was confirmed by broth microdilution, with an MIC of 6.25 µg/ml for *E. coli*, 12.5 µg/ml for *E. faecalis* and 25.0 µg/ml against both *S. aureus* and *P. aeruginosa*. The co-application of 100 µg/ml $disc^{-1}$ OFA01-AgNPs with standard antibiotic discs showed significant zone expansion (+5.5 mm to +10.5 mm; +23.9% to +95.5%) compared to antibiotic-alone baselines. The greatest improvement was seen with gentamicin against *E. faecalis* (+10.5 mm, +95.5%) and ampicillin against *S. aureus* (+10.0 mm, +83.3%). The results are in accordance with previously reported mechanisms that small (20–80 nm) sized biogenic AgNPs cause the disruption of membrane integrity and induce the production of ROS in the cells, which aids in the uptake of antibiotics .

Table 2: Dose-dependent antibacterial activity, MIC, and synergistic antibiotic potentiation of Talaromyces sp. OFA01-AgNPs against priority clinical pathogens

Test Organism	Gram Status	MIC (µg/ml)	Tested Antibiotic	Antibiotic Alone (mm)	Antibiotic + AgNPs (mm)	Zone Expansion (Δ mm)	Enhancement (%)	Outcome
S. aureus	G^+	25	Ampicillin (10 µg)	12.0±0.4	22.0±0.5	+10.0	+83.3%	Synergistic
E. faecalis	G^+	12.5	Gentamicin (120 µg)	11.0±0.3	21.5±0.4	+10.5	+95.5%	Synergistic
E. coli	G^-	6.25	Tetracycline (30 µg)	23.0±0.5	28.5±0.6	+5.5	+23.9%	Synergistic
P. aeruginosa	G^-	25	Ciprofloxacin (5 µg)	17.0±0.4	25.0±0.5	+8.0	+47.1%	Synergistic

3.5.5 Antifungal Potential and Comparative Synergism with Amphotericin B

OFA01-AgNPs also inhibited the mycelial proliferation of *Fusarium oxysporum* and *Alternaria alternata* in a dose-dependent fashion in a PPA disc-diffusion assay, producing inhibition zones comparable to those produced by reference 25 µg amphotericin B discs. The antidermatophytic performance aligns with the broad antifungal spectrum of *T. stipitatus* AgNPs against *F. oxysporum*, *A. alternata*, *Aspergillus flavus*, and *A. niger* , with the inhibition documented for *Alternaria* sp. AgNPs against phytopathogens , and with the antifungal bioactivity of peel-derived plant-extract AgNPs against *Fusarium*/*Alternaria* spp. . The data extend the antimicrobial envelope of biogenic AgNPs from the bacterial safety net to plant pathogen suppression—a critical contribution given that post-harvest losses attributable to *F. oxysporum* and *A. alternata* are massive worldwide .

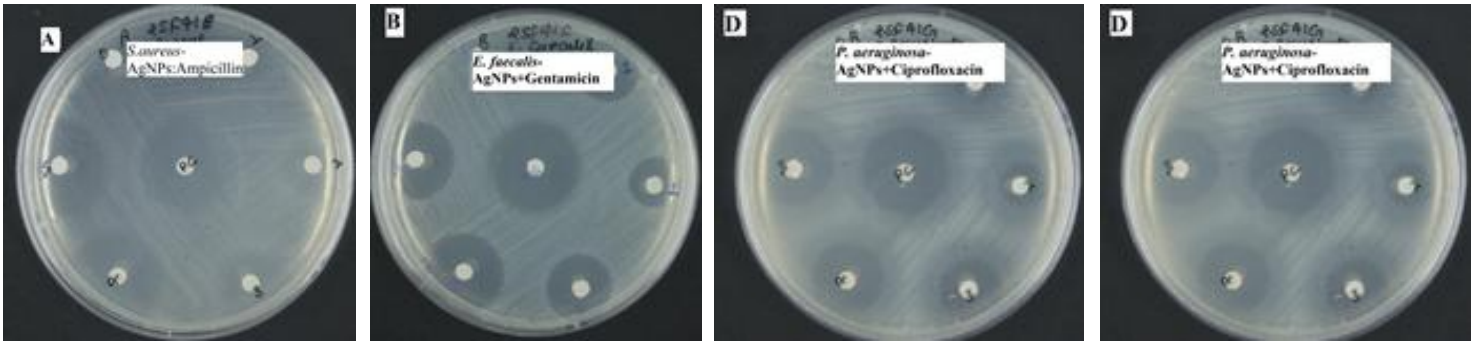

Fig. 5: Synergistic Effect of Standard Antibiotics against Potential Pathogenic Microbes
A) S. aureus, B) E. faecalis, C) E. coli, D) P. aeruginosa

CONCLUSION

The current research has successfully designed a cost-effective and eco-friendly approach by utilizing the composite four-peel (pomegranate/orange/mango/banana) agricultural waste as an isolation medium and cultivation broth for the green synthesis of silver nanoparticles by *Talaromyces* sp. OFA01 (GenBank: PX475677; 95.31% ITS identity to *Talaromyces* sp. XMSF-1). The developed approach comprising fungal isolation from fruit peel agar media, biomass growth in composite peel broth, secretome-mediated silver nanoparticle synthesis, physicochemical characterization, and antimicrobial activity appraisal was found to meet all the intended objectives of this study. The synthesized OFA01-AgNPs meet four important performance criteria for biogenic AgNP research: high colloidal stability, low crystalline domain size; Gram-negative preferring MICs (6.25–25 µg/mL), and a remarkable synergistic potentiation effect across four antibiotic classes (23.9% to +95.5%). In summary, the current study confirms that multi-fruit waste valorization is a profitable and environmentally friendly approach to obtaining valuable biogenic nanotherapeutics.

STATEMENTS AND DECLARATIONS

Ethical approval: This manuscript has not been published or presented elsewhere in part or in entirety and is not under consideration by another journal. All the authors have approved the manuscript and agree with submission to your esteemed journal. There are no conflicts of interest to declare. This article does not contain any studies with human participants or animals performed by any of the authors.

Conflict of interest: The authors declare that they have no conflict of interest.

References

1. Osman AI, Zhang Y, Farghali M, Rashwan AK, Eltaweil AS, El-Monaem EMA, Mohamed IMA, Badr MM, Ihara I, Rooney DW, Yap P. Synthesis of green nanoparticles for energy, biomedical, environmental, agricultural, and food applications: A review. Environmental Chemistry Letters 2024;22:841–87. https://doi.org/10.1007/s10311-023-01682-3.
2. Deeb BAE, Faheem GG, Bakhit MS. Biosynthesis of silver nanoparticles by Talaromyces funiculosus for therapeutic applications and safety evaluation. Scientific Reports 2025;15:13750–13750. https://doi.org/10.1038/s41598-025-95899-7.
3. Bhatnagar SS, Kobori T, Ganesh D, Ogawa K, Aoyagi H. Biosynthesis of Silver Nanoparticles Mediated by Extracellular Pigment from Talaromyces purpurogenus and Their Biomedical Applications. Nanomaterials 2019;9:1042–1042. https://doi.org/10.3390/nano9071042.
4. Kifle DR, Bacha K, Gonfa G. Antimicrobial activities of biosynthesized nanosilver using Musa paradisiaca and Citrus sinensis peel extracts against major human and plant pathogens. Scientific Reports 2025;15:6600–6600. https://doi.org/10.1038/s41598-025-91020-0.
5. Suhag R, Kumar R, Dhiman A, Sharma A, Prabhakar PK, Gopalakrishnan K, Kumar R, Singh A. Fruit peel bioactives, valorisation into nanoparticles and potential applications: A review. Critical Reviews in Food Science and Nutrition 2022;63:6757–76. https://doi.org/10.1080/10408398.2022.2043237.
6. Kamradgi S, Babanagare S, Gunagambhire VM. Characterization of Talaromyces islandicus–mediated silver nanoparticles and evaluation of their antibacterial and anticancer potential. Microscopy Research and Technique 2022;85:1825–36. https://doi.org/10.1002/jemt.24044.
7. Chavan A, Mavlankar GR, Baikar PP, Sah PM, Mourya N, Tirmali PM, Kakde UB. Pigment mediated biosynthesis of crystalline silver nanostructures: Structural characterization and enhanced multifunctional bioactivity. Next Nanotechnology 2026;9:100364–100364. https://doi.org/10.1016/j.nxnano.2026.100364.
8. Hu X, Saravanakumar K, Jin T, Wang M. Mycosynthesis, characterization, anticancer and antibacterial activity of silver nanoparticles from endophytic fungus *Talaromyces purpureogenus*. International Journal of Nanomedicine 2019:3427–38. https://doi.org/10.2147/ijn.s200817.
9. Bhat RS, Al-Dbass A, Khayyat AIA, Al-Daihan S. Utilizing Biomolecule-Rich Citrus Fruit Waste as a Medium for the Eco-Friendly Preparation of Silver Nanoparticles with Antimicrobial Properties. Inorganics 2024;12:180–180. https://doi.org/10.3390/inorganics12070180.
10. Xing Y, Liao X, Liu X, Li W, Huang R, Tang J, Xu Q, Li X, Yu J. Characterization and Antimicrobial Activity of Silver Nanoparticles Synthesized with the Peel Extract of Mango. Materials 2021;14:5878–5878. https://doi.org/10.3390/ma14195878.
11. Vigneswari S, Amelia TSM, Hazwan MH, Mouriya GK, Bhubalan K, Abdullah AA, Ramakrishna S. Transformation of Biowaste for Medical Applications: Incorporation of Biologically Derived Silver Nanoparticles as Antimicrobial Coating. Antibiotics 2021;10:229–229. https://doi.org/10.3390/antibiotics10030229.
12. Barapatre A, Aadil KR, Jha H. Synergistic antibacterial and antibiofilm activity of silver nanoparticles biosynthesized by lignin-degrading fungus. Bioresources and Bioprocessing 2016;3. https://doi.org/10.1186/s40643-016-0083-y.
13. Response Surface Method for Optimizing the Biosynthesis of Silver Nanoparticles Using Talaromyces stipitatus and Their Antimicrobial Activity. Jordan Journal of Biological Sciences 2022;15:511–22. https://doi.org/10.54319/jjbs/150321.
14. Guilger-Casagrande M, Lima R de. Synthesis of Silver Nanoparticles Mediated by Fungi: A Review. Frontiers in Bioengineering and Biotechnology 2019;7:287–287. https://doi.org/10.3389/fbioe.2019.00287.
15. Banerjee K, Ravishankar V. A Review on Mycosynthesis, Mechanism, and Characterization of Silver and Gold Nanoparticles. BioNanoScience 2017;8:17–31. https://doi.org/10.1007/s12668-017-0437-8.
16. Dadayya M, Thippeswamy MG, Shivaiah N, Veeranna SH, Gurubasajar N, Subhakar A, Thippeswamy B. Biological Potential of Silver Nanoparticles Synthesized by an Endophytic Fungus Metapochonia suchlasporia-KUMBMDBT-23. BioNanoScience 2023;13:1790–816. https://doi.org/10.1007/s12668-023-01177-z.
17. Soliman MKY, Salem SS, Abu-Elghait M, Azab MS. Biosynthesis of Silver and Gold Nanoparticles and Their Efficacy Towards Antibacterial, Antibiofilm, Cytotoxicity, and Antioxidant Activities. Applied Biochemistry and Biotechnology 2022;195:1158–83. https://doi.org/10.1007/s12010-022-04199-7.
18. Win TT, Khan S, Fu P. Fungus (Alternaria sp.) Mediated Silver Nanoparticles Synthesis, Characterization and Application as Phyto-Pathogens Growth Inhibitor. Research Square 2020. https://doi.org/10.21203/rs.3.rs-72789/v1.
19. Basheer MA, Abutaleb K, Abed NN, Mekawey AAI. Mycosynthesis of silver nanoparticles using marine fungi and their antimicrobial activity against pathogenic microorganisms. Journal of Genetic Engineering and Biotechnology 2023;21:127–127. https://doi.org/10.1186/s43141-023-00572-z.

20. Ghasemi S, Dabirian S, Kariminejad F, Koohi DE, Nemattalab M, Majidimoghadam S, Zamani E, Yousefbeyk F. Process optimization for green synthesis of silver nanoparticles using Rubus discolor leaves extract and its biological activities against multi-drug resistant bacteria and cancer cells. Scientific Reports 2024;14:4130–4130. https://doi.org/10.1038/s41598-024-54702-9.

21. Saied E, Abdel-Maksoud MA, Alfuraydi AA, Kiani BH, Bassyouni M, Al-Qabandi OA, Bougafa FHE, Badawy MSEM, Hashem AH. Endophytic Aspergillus hiratsukae mediated biosynthesis of silver nanoparticles and their antimicrobial and photocatalytic activities. Frontiers in Microbiology 2024;15:1345423–1345423. https://doi.org/10.3389/fmicb.2024.1345423.

22. Elamawi R, Al-Harbi RE, Hendi AA. Biosynthesis and characterization of silver nanoparticles using Trichoderma longibrachiatum and their effect on phytopathogenic fungi. Egyptian Journal of Biological Pest Control 2018;28. https://doi.org/10.1186/s41938-018-0028-1.

23. Guilger-Casagrande M, Germano-Costa T, Pasquoto-Stigliani T, Fraceto LF, Lima R de. Biosynthesis of silver nanoparticles employing Trichoderma harzianum with enzymatic stimulation for the control of Sclerotinia sclerotiorum. Scientific Reports 2019;9:14351–14351. https://doi.org/10.1038/s41598-019-50871-0.